

# Epistasis, core-genome disharmony, and adaptation in recombining bacteria

Aidan J. Taylor,<sup>1</sup> Koji Yahara,<sup>2</sup> Ben Pascoe,<sup>3</sup> Seungwon Ko,<sup>3</sup> Leonardos Mageiros,<sup>4,5</sup> Evangelos Mourkas,<sup>3</sup> Jessica K. Calland,<sup>6</sup> Santeri Puranen,<sup>7</sup> Matthew D. Hitchings,<sup>4</sup> Keith A. Jolley,<sup>3</sup> Carolin M. Kobras,<sup>8</sup> Sion Bayliss,<sup>9</sup> Nicola J. Williams,<sup>10</sup> Arnoud H. M. van Vliet,<sup>11</sup> Julian Parkhill,<sup>12</sup> Martin C. J. Maiden,<sup>3</sup> Jukka Corander,<sup>7,8,13</sup> Laurence D. Hurst,<sup>5</sup> Daniel Falush,<sup>14</sup> Paul Keim,<sup>3,15,16</sup> Xavier Didelot,<sup>17</sup> David J. Kelly,<sup>18</sup> Samuel K. Sheppard<sup>3</sup>

**AUTHOR AFFILIATIONS** See affiliation list on p. 15.

**ABSTRACT** Recombination of short DNA fragments via horizontal gene transfer (HGT) can introduce beneficial alleles, create genomic disharmony through negative epistasis, and create adaptive gene combinations through positive epistasis. For non-core (accessory) genes, the negative epistatic cost is likely to be minimal because the incoming genes have not co-evolved with the recipient genome and are frequently observed as tightly linked cassettes with major effects. By contrast, interspecific recombination in the core genome is expected to be rare because disruptive allelic replacement is likely to introduce negative epistasis. Why then is homologous recombination common in the core of bacterial genomes? To understand this enigma, we take advantage of an exceptional model system, the common enteric pathogens *Campylobacter jejuni* and *C. coli* that are known for very high magnitude interspecies gene flow in the core genome. As expected, HGT does indeed disrupt co-adapted allele pairings, indirect evidence of negative epistasis. However, multiple HGT events enable recovery of the genome's co-adaption between introgressing alleles, even in core metabolism genes (e.g., formate dehydrogenase). These findings demonstrate that, even for complex traits, genetic coalitions can be decoupled, transferred, and independently reinstated in a new genetic background—facilitating transition between fitness peaks. In this example, the two-step recombinational process is associated with *C. coli* that are adapted to the agricultural niche.

**IMPORTANCE** Genetic exchange among bacteria shapes the microbial world. From the acquisition of antimicrobial resistance genes to fundamental questions about the nature of bacterial species, this powerful evolutionary force has preoccupied scientists for decades. However, the mixing of genes between species rests on a paradox: On one hand, promoting adaptation by conferring novel functionality; on the other, potentially introducing disharmonious gene combinations (negative epistasis) that will be selected against. Taking an interdisciplinary approach to analyze natural populations of the enteric bacteria *Campylobacter*, an ideal example of long-range admixture, we demonstrate that genes can independently transfer across species boundaries and rejoin in functional networks in a recipient genome. The positive impact of two-gene interactions appears to be adaptive by expanding metabolic capacity and facilitating niche shifts through interspecific hybridization. This challenges conventional ideas and highlights the possibility of multiple-step evolution of multi-gene traits by interspecific introgression.

**KEYWORDS** *Campylobacter*, hybridization, epistasis, introgression, horizontal gene transfer, recombination, linkage disequilibrium

**Editor** Sebastian Suerbaum, LMU Munich, Munich, Germany

Address correspondence to David J. Kelly, d.kelly@sheffield.ac.uk, or Samuel K. Sheppard, samuel.sheppard@biology.ox.ac.uk.

The authors declare no conflict of interest.

See the funding table on p. 16.

**Received** 27 February 2024

**Accepted** 26 March 2024

**Published** 29 April 2024

Copyright © 2024 Taylor et al. This is an open-access article distributed under the terms of the [Creative Commons Attribution 4.0 International license](https://creativecommons.org/licenses/by/4.0/).

Mutation is the engine of genetic novelty, but for most bacteria, adaptation also involves the acquisition of DNA from other strains and species through horizontal gene transfer (HGT) (1). In some well-documented cases, a single-nucleotide substitution or acquisition of a small number of genes can prompt new evolutionary trajectories with striking outcomes such as the evolution of virulent or antibiotic-resistant strains (2). With such dynamic genomic architecture, it may be tempting (and possibly useful [3]) to consider genes as independent units that “plug and play” innovation into recipient genomes. This is clearly an oversimplification. In fact, genes within genomes are highly interactive wherein the effect of one allele depends on another (epistasis). Therefore, it is likely that some horizontally introduced changes will disrupt gene networks and be costly to the original coadapted genetic background, especially for complex phenotypes involving multiple genes and more distant taxonomic relationships.

Understanding how epistasis influences the evolution of phenotype diversity has preoccupied researchers since the origin of population genetics (4–10), with much emphasis placed upon the relative amounts of recombination and epistatic effect sizes (11, 12). In sexual populations, such as outbreeding metazoans, genetic variation is shuffled at each generation. This trend toward randomization between alleles (linkage equilibrium) means it is unlikely that multiple distinct epistatic allele combinations will be maintained in the same population (8). In bacteria, however, rapid clonal reproduction allows multiple genomically distant beneficial allele combinations to rise to high frequency or even become fixed in a single population. For example, in common enteric bacteria such as *Escherichia coli*, *Salmonella enterica*, and *Campylobacter jejuni*, the doubling time in the wild has been estimated at around 24 hours or less (13, 14). Therefore, though HGT occurs in these organisms (15), even in highly recombinogenic *C. jejuni* (13, 16), there will likely be many millions of bacterial generations between recombination events at a given locus. This allows mutations that are beneficial only in specific genetic backgrounds to establish in a single population and linkage disequilibrium (LD) to form between different epistatic pairs (16, 17).

In a coadapted genomic landscape, recombination is expected to have two antagonistic effects. On one hand, it could be beneficial, promoting adaptation by conferring novel functionality on the recipient genome (18–22) and, through specialization, reducing the competition between clones (clonal interference). On the other, it could be detrimental, introducing disharmonious allele combinations that will be discriminated against by selection (19). The balance of these two effects is likely to be different for core and non-core HGT events. Non-core events, such as introduced accessory antibiotic resistance genes, can be immediately beneficial, and as they do not replace recipient sequence, need not break established epistatic interactions. By contrast, HGT replacing one allele for another (homologous recombination) in part of the core genome is likely to disrupt highly evolved co-adapted networks. For these reasons, negative epistatic interactions between core genes with different evolutionary histories have been proposed as a barrier to recombination (4–10, 23), particularly between species. However, interspecies recombination is common in bacterial core genomes (18, 24–29). How then can a core genome, that is expected to build up extensive co-adapted epistatic networks, be so accepting of HGT events?

The common animal gut bacterium *Campylobacter*, which is among the most prolific causes of human bacterial gastroenteritis worldwide (30), provides an exceptional model system to study the impact of HGT on the core genome for several reasons. First, high levels of introgression have occurred between the two most important pathogenic species, *C. jejuni* and *C. coli*, this has led to the evolution of a globally distributed “hybrid” *C. coli* lineage (25) that is responsible for almost all livestock and human infections with this species. Identified as *C. coli* with numerous alleles of *C. jejuni* ancestry, the hybrids occupy a niche that was not available to the parental subtypes, suggesting that the introgressed genes provide an adaptive advantage (25, 26, 31). Second, up to 23% of the core genome of one common *C. coli* subtype has been recently introgressed from *C. jejuni* (26), potentially disrupting epistatic interactions. Finally, because *C. jejuni* and *C. coli*

have undergone an extended period of independent evolution with only 85% average nucleotide identity, recombined sequence is conspicuous in the genome.

Here, we investigate the disruptive effect of HGT on co-adapted bacterial core genomes by examining co-varying allele pairings and imported DNA sequence. Even though recombined fragments enter the genome one by one, we find that most covariation in the core genome is between sites where both alleles were imported. Having confirmed that allelic covariation is indicative of epistasis, with laboratory mutagenesis and complementation assays, we conclude that independent disruptive recombination events occur and persist until a second event restores the functional link in a new genetic background. Specifically, the first recombination had a negative fitness effect, which is why *C. jejuni*-*C. coli* allele combinations were rare, followed by a rescuing recombination at the other locus re-instating harmony. This process resembles the two-hit cancer model where an initial mutation is actuated by a second (32). Both bacterial and cancer cell lines are asexual clones, and a two-hit model for core genome HGT is consistent with a more general theory in which negative effects from an initial event (MGT or mutation) need not preclude adaptive evolution. As in cancer, the recombinant genotypes are under strong selection and occupy a unique agricultural niche.

## RESULTS

### ***Campylobacter* populations are highly structured with intermediate sequence clusters**

All unique genes were automatically annotated using the RAST/SEED platform (33), for 973 isolate genomes (827 *C. coli* and 146 *C. jejuni*, Data S4), and compared using BLAST to create a reference pan-genome list of all genes in all isolates (34). The presence of all unique genes was determined in isolate genomes by comparison to this pan-genome. This revealed a core genome of 631 gene orthologs in all *Campylobacter* isolates in this study. There were 1,287 genes common to all *C. jejuni* isolates and 895, 1,021, and 1,272 common to *C. coli* clades 1, 2, and 3, respectively. Consistent with previous studies (26), neighbor-joining and ClonalFrameML trees based on genes within concatenated core genome alignments revealed population structure in which *C. jejuni* and *C. coli* clade 2 and 3 isolates each formed discrete clusters (Fig. 1A; Fig. S1). Isolates designated as *C. coli* clade 1 were found in three clusters on the phylogeny: unintrogressed ancestral strains, and the ST-828 and ST-1150 clonal complexes (CCs) which account for the great majority of strains found in agriculture and human disease (26). Pan-genome analysis quantified the increase in unique gene discovery as the number of sampled genomes increased (Fig. S2A). For all phylogenetic clusters, there was evidence of an open pan-genome with a trend toward continued rapid gene discovery within clusters containing fewer isolates. There was considerable accessory genome variation between species and clades, potentially associated with important adaptive traits (Fig. S3), and there was evidence that the average number of genes per genome was greater in *C. coli* CC-828 isolates than in *C. jejuni* (Fig. S2B).

### **There is substantial introgression within the *C. coli* core genome**

The large genetic distances among *C. coli* clade 1 isolates (Fig. 1A) have been shown to be a consequence of the import of DNA from *C. jejuni* rather than accumulation of mutations during a prolonged period of separate evolution (25). Chromosome painting and FineStructure (35, 36) were used to identify DNA chunks from the donor *C. jejuni* population in recipient *C. coli* genomes. A co-ancestry matrix of genome-wide haplotype data was used to infer the co-ancestry of core-genome haplotype data from CC-828 and CC-1150 isolates. This gave a detailed representation of the recombination-derived segments from each *C. jejuni* donor group and clonal complex to each recipient individual (Fig. S4). The majority of introgressed SNPs were rare, occurring in fewer than 50 recipient genomes (Fig. 1B). However, a large proportion of the introgressed *C. coli* clade

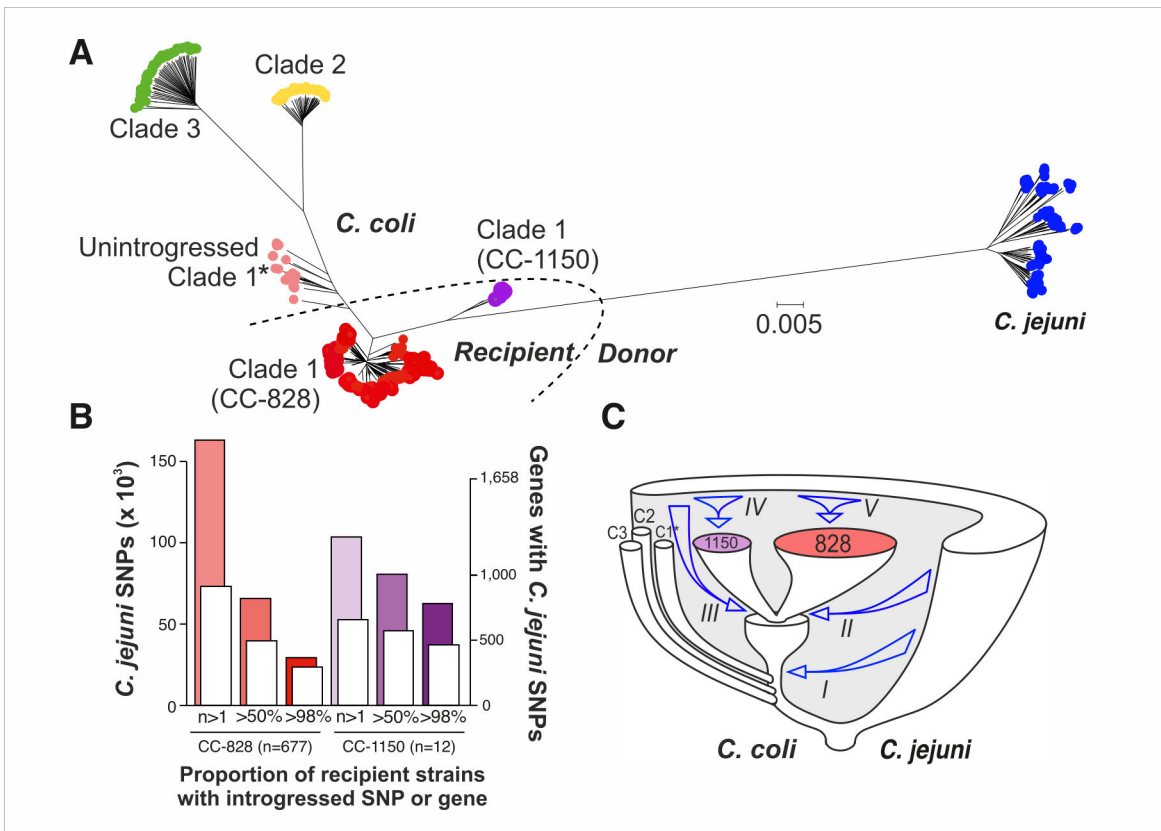


**FIG 1** Genome-wide introgression from *C. jejuni* to *C. coli*. (A) Phylogenetic tree reconstructed using neighbor-joining method on a whole-genome alignment of 973 *C. jejuni* and *C. coli* isolates. Introgressed *C. coli* clades are represented with red (CC-828,  $n = 677$ ) and purple (CC-1150,  $n = 12$ ) circles, unintegrated clade 1\* ( $n = 35$ ) is shown in pink, clade 2 ( $n = 45$ ) in yellow, and clade 3 ( $n = 58$ ) in green. A set of 146 *C. jejuni* genomes belonging to 30 clonal complexes (4 to 5 isolates per ST) are shown in blue. Recipient and donor populations, used to infer introgression in chromosome painting analysis, are indicated. The scale bar represents the number of substitutions per site. (B) Summary of introgressed *C. jejuni* SNPs in *C. coli* CC-828 ( $n = 677$ , red) and CC-1150 ( $n = 12$ , purple) genomes using ChromoPainter; the number of introgressed core SNPs (colored histograms; left y-axis) and core genes (white histograms; right y-axis) for a range of recipient strain proportions (at least 1, more than 50% and more than 98%) is shown. (C) Diagram of *Campylobacter* species and clade (C1\*, C2, C3) divergence with arrows indicating sequential introgression from *C. jejuni* into *C. coli* (I) clade 1, (II, III) CC-828 and CC-1150, (IV, V) subsequent clonal expansion and ongoing introgression.

1 genomes contained DNA of *C. jejuni* ancestry in >98% of recipient isolates. Consistent with previous estimates (26), these regions where introgressed DNA was found in almost all introgressed *C. coli* strains occurred across the genome and comprised up to 15% and 28% of the CC-828 and CC-1150 isolate genomes, respectively (Fig. 1B). The majority of introgressed DNA in *C. coli* involves genes that are present in multiple *C. jejuni* lineages (core genes) (Fig. S5A).

Having identified *C. jejuni* ancestry within *C. coli* genomes, we investigated the sequence of events responsible for introgression. Most introgressed SNPs are found at low frequency in both CC-828 and CC-1150 clonal complexes. However, there was evidence of SNPs that are introgressed in both complexes as well as high-frequency lineage-specific introgression in both CC-828 and CC-1150 (Fig. S5B). Specifically, 25% of the *C. jejuni* DNA found in >98% of CC-828 isolates was also found in CC-1150 (Fig. S5C), implying that this genetic material was imported by the common ancestor(s) of both complexes. After the divergence of these two complexes, introgression continued with nearly 75% of *C. jejuni* DNA present in one recipient clonal complex and not the other. This stepwise model is consistent with an evolutionary history in which there was a period of progressive species and clade divergence reaching approximately 12% at the nucleotide level between *C. jejuni* and *C. coli* and around 4% between the three *C. coli* lineages. More recently, changes to the patterns of gene flow led one *C. coli* clade

1 lineage to import substantial quantities of *C. jejuni* DNA, and further lineage-specific introgression gave rise to two clonal complexes (CC-828 and CC-1150) that continued to accumulate *C. jejuni* DNA, independently creating the population structure observed today (Fig. 1C).

The high magnitude introgression into *C. coli* clade 1 isolates has introduced thousands of nucleotide changes to the core genome. However, divergence in bacteria may be uneven across the genome for at least two reasons. First, recombination is more likely to occur in regions where donor and recipient genomes have high nucleotide similarity (24, 37, 38). Second, “fragmented speciation” (39), in which gene flow varies in different parts of the genome, such as regions responsible for adaptive divergence, can result in phylogenetic incongruence among genes. Consistent with previous estimates (26), we found that the three *C. coli* clades had similar high divergence with *C. jejuni* across the genome, ranging from 68% to 98% nucleotide identity for individual genes (Fig. S5D), implying a period of divergence with low levels of gene flow. We found no evidence that high genetic differentiation between the species prevented recombination. While there was some evidence that more recombination occurred in regions of low nucleotide divergence (between unintrogressed *C. coli* clade 1 and *C. jejuni*), introgression occurred across the genome at sites with a wide range of nucleotide identity (Fig. S5D). This level of recombination has greatly increased overall genetic diversity across the genome in *C. coli* clade 1 and introduced changes that have potential functional significance.

### Much of the putative epistasis occurs between SNPs in introgressed genes

ClonalFrameML (40) was used to quantify recombination within the genomes, based on SNP density, and produce a corrected tree that accounted for the effect of recombination and inferred the ancestral sequence of each node. These analyses revealed the importance of homologous recombination in generating sequence variation within the introgressed *C. coli*. Estimates of the relative frequency of recombination versus mutation ( $R/\theta = 0.43$ ), mean recombination event length ( $\delta = 152$  bp), and average amount of polymorphism per site in recombined fragments ( $v = 0.07$ ) imply that recombination has had an effect ( $r/m$ ) 4.57 times higher than *de novo* mutation during the diversification of CC-828. This is consistent with previous analysis and confirmed recombination as the major driver of molecular evolution in *C. coli* (13, 26, 41).

Covariation analysis identified SNP combinations in independent genetic backgrounds by accounting for the sequence variation associated with the inferred phylogeny. The continuous time Markov chain (CTMC) model was used to investigate the joint evolution of pairs of biallelic sites on a phylogenetic tree. Parameters ( $\alpha_1$ ,  $\alpha_2$ ,  $\beta_1$ , and  $\beta_2$ ) were estimated for independent substitutions for pairs of sites ( $ab$ ,  $Ab$ ,  $aB$ , and  $AB$ ) across the genomes, and substitution rates were determined (Fig. S6). This was applied to investigate patterns of covariance for all pairs of sites >20 kbp apart (Fig. S7). For most biallelic sites, there were few branches on the tree where substitutions occurred so that their evolution is compatible with separate evolution on the same clonal frame. However, 2,874 co-varying pairs evolved more frequently together than would be expected ( $P$ -value  $10^{-8}$ ) if they had evolved independently based on the tree, and hence, indicated patterns of putative epistasis.

Among them, the location of 2,618 putative epistatic pairs of sites was compared to the inferred ancestry (unintrogressed *C. coli* or *C. jejuni*) of sequence across the genome of CC-828 and CC-1150 *C. coli* strains (Fig. 2C; Data S1). Putative epistatic pairs in the recipient introgressed genome represent a combination of the haplotypes in the ancestral populations (Fig. 2A). For each epistatic pair, the major and minor haplotypes were defined, from these possible combinations, if there was haplotype polymorphism between *C. jejuni* and *C. coli*. This allowed quantification of the number of co-varying sites that occurred between an ancestral *C. coli* (unintrogressed) and an introgressed *C. jejuni* allele (*C. coli*-*C. jejuni*), two introgressed alleles (*C. jejuni*-*C. jejuni*), and sites that do not segregate by species. Strikingly, the breakdown of the major and

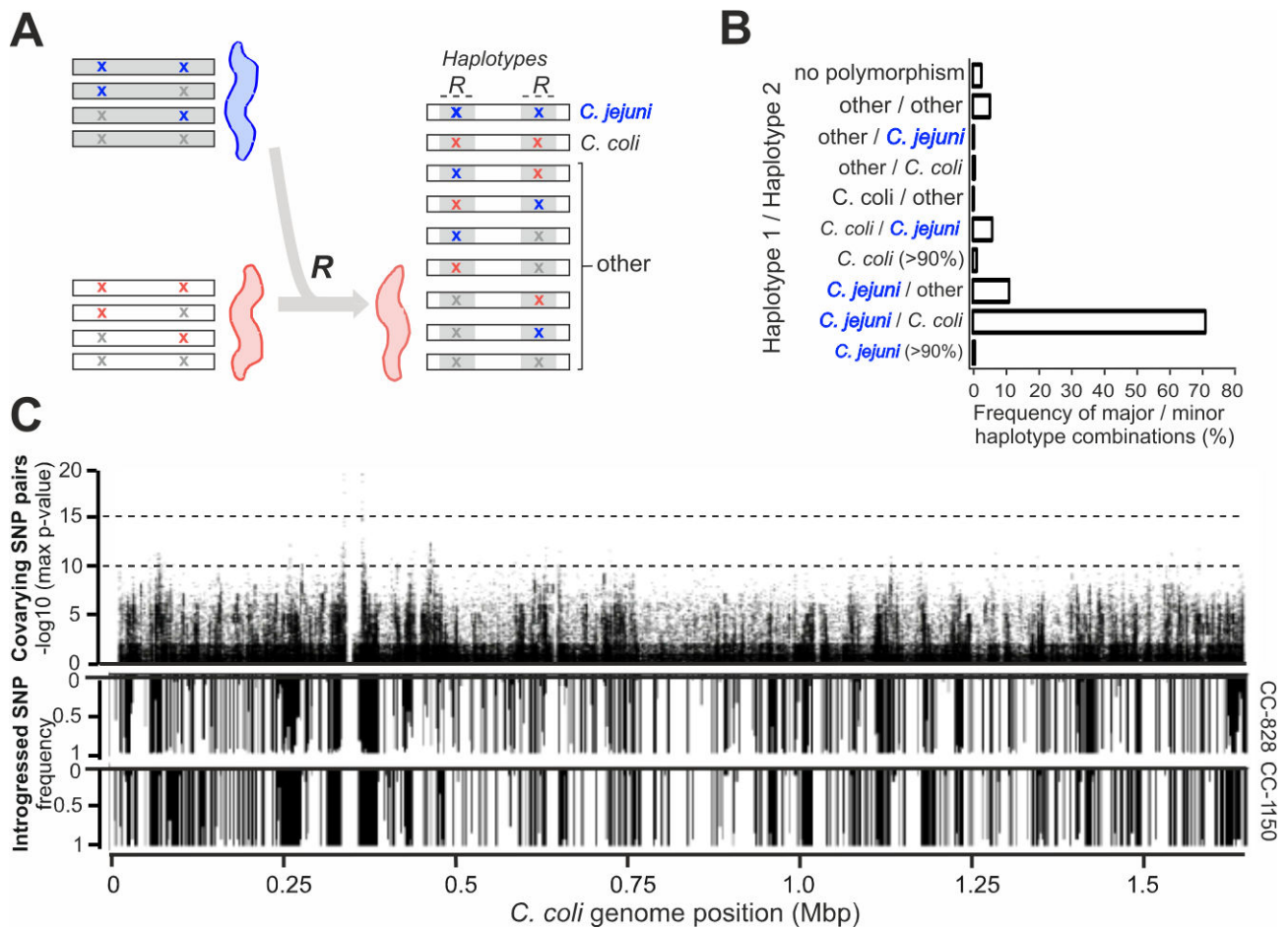


**FIG 2** Covariation in introgressed *C. coli* genomes. (A) Possible SNP pairs in ancestral donor *C. jejuni* and recipient *C. coli* genomes and potential recombinant (*R*) haplotype pairs in introgressed *C. coli*. Possible genome haplotypes are designated with *C. jejuni*-fixed SNPs (blue X), other *C. jejuni* SNP (gray X), *C. coli*-fixed SNP (red X), and other *C. coli* SNPs (gray X). (B) The frequency of major and minor haplotype combinations among the 2,578 pairs of co-varying SNPs in the 689 *C. coli* clade-1-recipient genomes, revealing that 83.5% of long-range covariation was between introgressed *C. jejuni* sites. (C) Miami plot of each polymorphic site showing the maximum *P*-value for co-varying biallelic pairs (>20 kbp apart) and the frequency of introgression in CC-828 and CC-1150.

minor haplotype combinations among the 2,618 epistatic pairs (Fig. 2B; Data S2) shows the major haplotype for 83.5% of putative epistatic SNP pairs was *C. jejuni*, indicating that both co-varying sites had *C. jejuni* ancestry, consistent with epistasis between introgressed ancestral *C. jejuni* sequence at divergent genomic positions. Investigation of the genes containing co-varying sites revealed that 2,187 SNP pairs were in 16 genes with just 5 genes accounting for 99.1% of them (Fig. 3 and Fig. 4A and B; Data S3). Linkage disequilibrium decay was calculated as a function distance between co-varying SNPs in the CVM29710 reference genome showing decreasing mean  $R^2$  to a stable value of 0.03–0.07 after approximately 5,000 bp (Fig. 3B). High LD was observed among 12 putatively epistatic *C. jejuni*-*C. jejuni* SNP pairs indicating strong linkage (covariation) between alleles.

### Genomic context and physiological role of epistatically linked genes

The five genes accounting for the majority of epistatic interactions (*cj1167*, *cj1168c*, *cj1171c/ppi*, *cj1507c/modE*, and *cj1508c/fdhD*) were investigated for their physiological role in *C. jejuni*. FdhD and ModE are proteins involved in the biogenesis of formate dehydrogenase (FDH). The FDH complex (FdhABC) oxidizes formate to bicarbonate to generate electrons that fuel cellular respiration. Formate is an abundant electron donor produced by host microbiota and an important energy source for *Campylobacter in vivo*

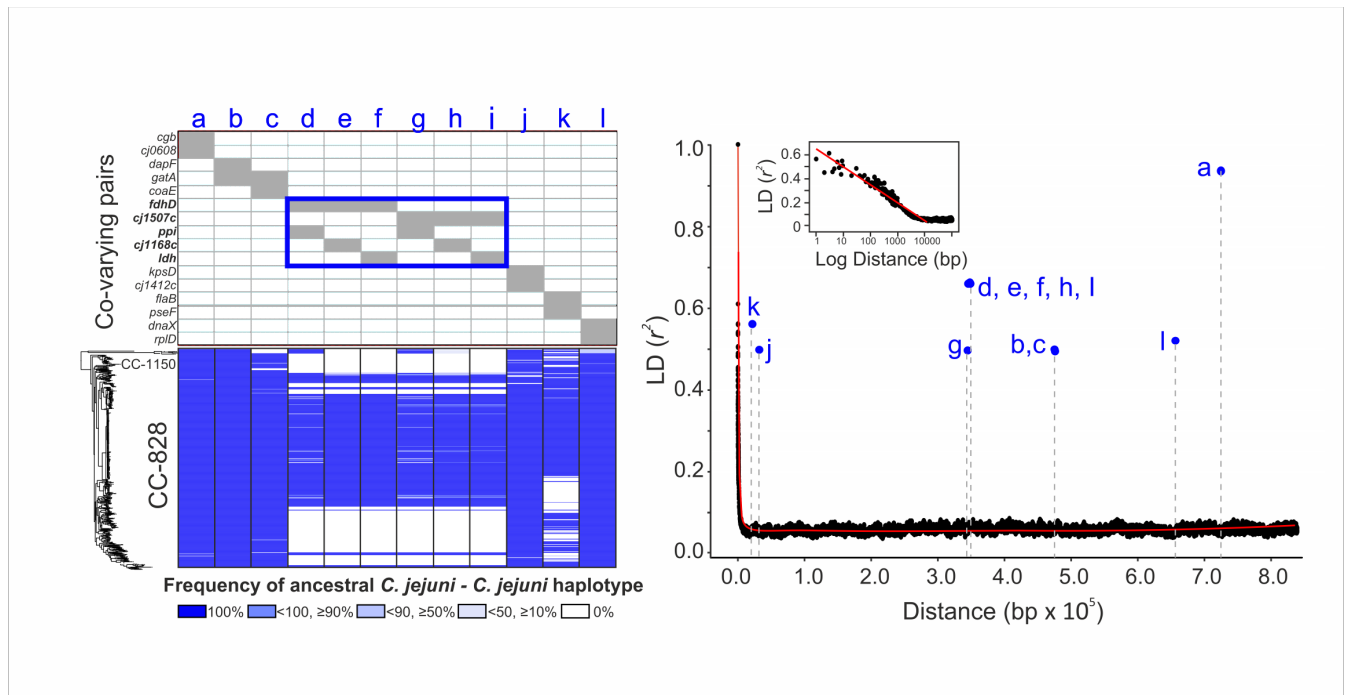


**FIG 3** Putative epistatic SNP pairs in introgressed *C. coli* genomes where the major haplotype was *C. jejuni*, indicating that both co-varying sites had *C. jejuni* ancestry. (Left) A total of 16 gene pairs in which the *C. jejuni*-*C. jejuni* haplotype is dominant (a to l), and frequency of ancestral *C. jejuni*-*C. jejuni* haplotype among the epistatic SNP pairs in co-varying genes is shown as the 5 categories for each *C. coli* strain mapped to the phylogeny (ML tree). Shades of blue indicate the % of the epistatic SNPs in the co-varying gene with ancestral *C. jejuni*-*C. jejuni* haplotype. (Right) Linkage disequilibrium ( $r^2$ ) decay across the *C. coli* CVM29710 reference genome calculated by comparison of 690 *C. coli* isolate genomes (ST-828 and ST-1150, Data S4). LD is determined between SNP pairs, and average LD is shown for 100 bp blocks (black dots). A red trendline plots average LD. The inset is the same data plotted on a log scale, showing that LD remains approximately constant after 5 kbp. The position of 12 co-varying *C. jejuni*-*C. jejuni* SNP pairs (blue dots) is plotted (a to l).

(42, 43). Therefore, attenuated function of FDH would be highly likely to reduce fitness *in vivo*. The remaining three genes, *cj1167* (annotated incorrectly as *ldh*, lactate dehydrogenase), *cj1168c*, and *cj1171c* (*ppi*) are also grouped together in the genome, where *cj1167* and *cj1168c* are adjacent but with the open reading frames convergent and overlapping, while *ppi* is upstream, separated by two non-epistatically linked genes (*cj1169c* and *cj1170c*, Fig. 4B). Considering the genomic arrangement, it is therefore clear that the putative epistatic links uncovered in this study essentially occur across two loci in the genome (*fdhD/modE* and *cj1167/cj1168c/ppi*), with each of the latter three genes linked with both *fdhD* and *modE* (Fig. 4B). Given the known function of *fdhD* and *modE* in biogenesis of the FDH complex, we hypothesized that *cj1167/cj1168c/ppi* might also have some role in FDH biogenesis or activity in order to form a functional epistatic connection. We therefore constructed deletion mutants to investigate the possible role of these genes in FDH activity. Specifically, *cj1167* and *cj1168c* (*selF*), *cj1171c* (*ppi*), *cj1507c* (*modE*), *cj1508c* (*fdhD*), and *cj1500* (*fdhT*) were deleted by gene replacement mutagenesis, with the majority of the open reading frame replaced by an antibiotic resistance cassette.

Initially, each of the mutants and their parental wild type (*C. jejuni* NCTC11168) were grown in rich media (Muller-Hinton [MH] broth), and their formate-dependent oxygen consumption rates determined (Fig. 4C). *cj1167*, *cj1168c*, and *ppi* mutants demonstrated wild-type levels of FDH activity, while activity in both *fdhD* and *modE* mutants was abolished. To confirm that the phenotype of the *fdhD* and *modE* mutants was not due to a polar effect on the surrounding *fdh* locus, these mutants were genetically complemented by reintroduction of a second copy of the wild-type gene into the rRNA locus, which restored near wild-type levels of FDH activity in both cases (Fig. 4C).

As neither *cj1167*, *cj1168c*, nor *ppi* mutants showed altered FDH activity in cells grown in rich media, we considered that their function may be related to an FDH-specific

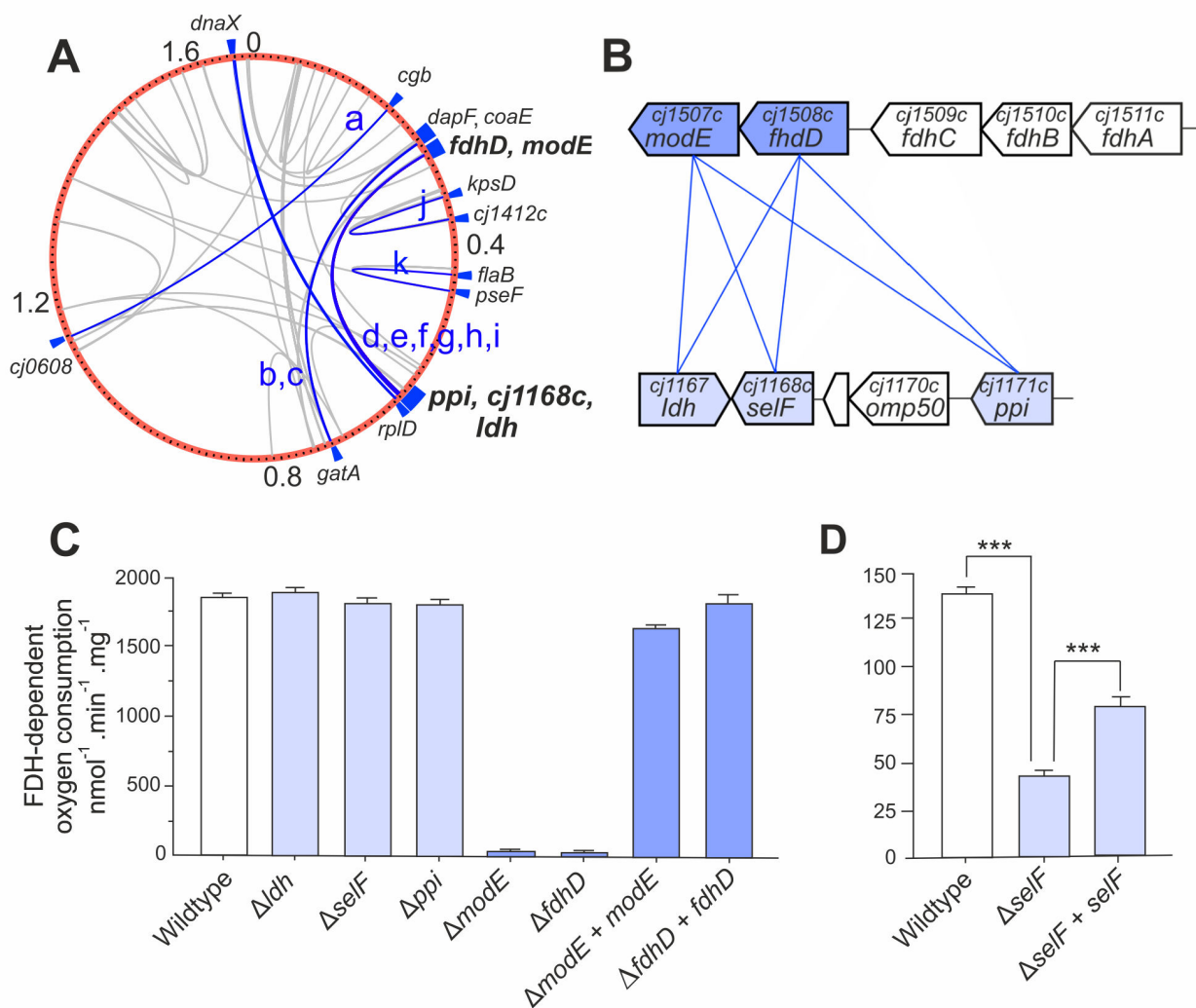


**FIG 4** Genomic context and physiological roles of introgressed epistatically linked genes involved in FDH biogenesis and activity. (A) The position of putative epistatic sites mapped on the *C. coli* CVM29710 reference for co-varying *C. jejuni*-*C. jejuni* SNPs (blue) in 16 gene pairs (a to l) and other haplotype combinations (gray). (B) Genome organization of the most common co-varying introgressed *C. jejuni*-*C. jejuni* gene pairs linked to FDH. (C and D) FDH activity of whole cells determined by oxygen consumption rates in a Clark-type electrode (nanomoles of oxygen consumed per minute per milligram of total protein) for (C) cells grown in rich media (excess selenium) and (D) cells grown in minimal media with 0.5 nM sodium selenite. \*\*\* denotes *P* value of <0.001 by Student's *t*-test.

nutrient requirement as would likely be found *in vivo*. Since the formate-oxidizing subunit of FDH, FdhA, specifically requires a molybdo- or tungsto-pterin (Mo/W) cofactor and a selenocysteine (SeC) residue for catalysis (44), Mo, W, or Se supply presented possible targets. *cj1168c* encodes a DedA family integral membrane protein of unknown function. DedA proteins are solute transporters widespread in bacteria but are mostly uncharacterized (45). However, a homolog of *cj1168c* in the heavy metal specialist beta-proteobacterium *Cupriavidus metallidurans* has been shown to be involved in selenite (SeO<sub>3</sub><sup>2-</sup>) uptake (46). We therefore speculated that Cj1168 could be a selenium oxyanion transporter that supplies Se for SeC biosynthesis. To test this, FDH activities were measured in *cj1168c* mutant and parental wild-type strains grown in minimal media with limiting concentrations of selenite or selenate (SeO<sub>4</sub><sup>2-</sup>) (Fig. S9). The data in Fig. 4D show that the *cj1168c* mutant displayed significantly reduced FDH activity after growth with selenite in the low nanomolar range, and this phenotype was partially restored by genetic complementation. We therefore designated *cj1168c* as *self* (selenium transporter for formate dehydrogenase). However, although this phenotype does suggest that Self is



a selenium importer, another unrelated selenium transporter, FdhT (Cj1500), has previously been documented in *C. jejuni* (47), which is not epistatic with *fdhD* or *modE*. In contrast to this previous report, we found considerable residual FDH activity still remained in an *fdhT* deletion mutant, which was fully restored to wild-type levels by complementation (Fig. S8).

Finally, we tested whether the residual FDH activity in our *fdhT* mutant was due to selenium uptake by Self. An *fdhT self* double mutant was generated and assayed for FDH activity after growth in minimal media containing limiting concentrations of selenite or selenate (Fig. S8). The *fdhT self* double mutant demonstrated a significant additional reduction in FDH activity over the *fdhT* single mutant, a phenotype that was partially restored by complementing the double mutant with *self*. Complementation of the double mutant with *fdhT* returned FDH activity to near wild-type levels (Fig. S8). Taken together, our data suggest that both FdhT and Self facilitate selenium acquisition in *C. jejuni*, possibly representing low- and high-affinity transporters, respectively (Fig. S10).

## DISCUSSION

To address the apparent contradiction of frequent core genome recombination in a co-adapted genomic background, we focused on *Campylobacter*, in which interspecies recombination is well documented (25, 26, 48). As in other studies, we found that a large proportion (15%–28%) of the *C. coli* core genome originated in *C. jejuni* despite the genetic dissimilarity (~85% nucleotide identity) between the species. Investigating the likely disruptive impact this would have on co-adapted epistatic gene networks, we quantified the frequency of *C. jejuni-C. coli* (and *vice versa*) and *C. jejuni-C. jejuni* co-varying allele pairs in introgressed *C. coli*. Where recombination is minimally disruptive, there would be more *C. jejuni-C. coli* than *C. jejuni-C. jejuni*. However, consistent with selection against disharmonious gene combinations, we found that *C. jejuni-C. jejuni* allele pairs constituted >83% of co-varying introgressed haplotypes.

There are different explanations for the overrepresentation of *C. jejuni-C. jejuni* allele pairs in introgressed *C. coli* genomes. First, in a large HGT event model, it is possible that both co-varying sites were introgressed in a single large recombination event (49–51). However, in *Campylobacter*, LD decreases with distance for pairs of sites and is approximately constant after 5 kbp (52). This means that it is highly unlikely that the introgressed genes arrive in recipient genome in single large events and suggests the independent acquisition of alleles that are >20 kbp apart. Second, in small HGT event accumulation model, introgressed genes would have little impact and build up in the recipient genome over time. If this were true, many pairings would be between solitary introgressed *C. jejuni* alleles and *C. coli* alleles in the recipient genome. However, sites where the major haplotype combination was *C. jejuni-C. coli* (“other” on Fig. 2B; Data S2) represent just 6% putative epistatic allele pairings. Finally, in a two-hit epistasis model, the first introgressed *C. jejuni* allele is disruptive but not fatal to the recipient *C. coli* genome, hence, the relative scarcity of *C. jejuni-C. coli* allele pairings. A second introgression event then restores, or enhances, the function of the integrated *C. jejuni-C. jejuni* coevolutionary unit.

Statistical genetic analysis confirmed covariation, but to confirm coadaptation (*sensu stricto*), it was necessary to confirm epistasis in the laboratory. The most common co-varying *C. jejuni-C. jejuni* gene pairs were linked to FDH, a key enzyme allowing the utilization of formate as an electron donor *in vivo* (42, 43). FdhD and ModE were shown to be essential for FDH activity. While FdhD is a known sulfur-transferase required for cofactor insertion into FdhA (53) (Fig. S11), the abolished FDH activity in an *modE* mutant indicates functions for ModE in FDH biogenesis, beyond the known role as a transcriptional repressor (54, 55). In contrast, *cj1167*, *self*, and *ppi* mutants did not show reduced FDH activity. This apparently contradicted the epistasis hypothesis until we considered the functional links between *fdhD/modE* and *cj1167/self/ppi*. This revealed that a *self* mutant strain had significantly reduced FDH activity under conditions of

selenite limitation (Fig. 4D). This phenotype is consistent with SelF being a high-affinity Se oxyanion transporter and functionally links SelF with FdhD/ModE. Therefore, we suggest that *selF* rather than *fdhT* is epistatic because SelF confers an additional benefit (SeC biosynthesis, essential for FDH activity) under conditions of selenium limitation, for example, as may be found in the host gut (Fig. S10). The conventional diet of broiler chickens is considered selenium limited, as dietary supplementation improves weight gain, antioxidant activity, gut health, and tissue-specific deposition of selenium (56–58). The intestinal niche of broiler chickens inhabited by *Campylobacter* spp. is therefore likely to be selenium limited without diet supplementation: a relatively recent practice following recommendations from the NRC in 1994 (59, 60).

Direct functional association with FDH activity was more difficult to explain for *cj1167* and *ppi*. *cj1167* is currently incorrectly annotated as lactate dehydrogenase (Ldh), and its actual function is unknown (61). While we found no evidence for a functional connection between Cj1167 and FDH activity, the overlapping convergent gene arrangement of *cj1167* and *cj1168c* (*selF*) suggests a transcriptional architecture that might form similar epistatic dependencies even if Cj1167 is not required for FDH activity. Finally, the *cj1171c* (*ppi*) deletion mutant showed no growth defect or reduction in FDH activity. *ppi* encodes a cytoplasmic peptidyl-prolyl *cis-trans* isomerase, and PPlases are general protein-folding catalysts that often have pleiotropic and redundant functions (62). Therefore, it is possible that Cj1171 does help promote the folding of FdhD or ModE, but analysis of a simple deletion mutant may not reveal this if another PPlase can substitute in that genetic background.

Understanding the functional significance of core genome recombination has considerable potential to explain the evolution of complex phenotypes. In *Campylobacter*, our results suggest that an ancestral *C. coli* lineage colonized a new niche, and surviving lineages (CC-828 and CC-1150) gained access to *C. jejuni* DNA (Fig. 5A and B). In this case, introgressed *C. coli* acquired multiple genes allowing them to utilize the high levels of formate in the host gut as an energy source. Specifically, the *fdhD* and *ModE*, essential for FDH biogenesis, as well as *selF* that ensures sufficient selenium for the enzyme to function in selenium-limited conditions as likely occur in the broiler chicken gut. This example shows how as the adaptive landscape of the genome changed, potentially decoupling epistatic interactions that were previously selected, new gene combinations can be introduced by homologous recombination and tested in the *C. coli* genetic background. These new recombinant genotypes are frequently isolated in the agricultural setting and from clinical cases caused by agricultural products, arguing for their enhanced fitness in this niche.

The notion that multiple events are necessary to achieve a phenotype with the first event potentially being deleterious (inferred to cause negative epistasis) is strongly reminiscent of the two-hit cancer model in eukaryotes (32) in which the benefit to the tumor cell appears only after earlier non-advantageous mutations. In bacteria, while the first hit (HGT event) in a core genome is consistent with fitness costs associated with putative negative epistasis (breaking co-adapted gene networks), this can be rescued by a second HGT event. The second event, in effect, restores a pre-existing co-adapted allele pair from the donor species to the recipient. This type of genetic rewiring may indeed be more common than previously thought (63–65), and despite theoretical expectations, negative epistasis is not an absolute barrier to genome-wide recombination in structured bacterial populations. Multiple HGT events thus provide a solution to the classic evolutionary fitness peak jumping problem and, of course, occur in a dynamic environment with a many changing subniche.

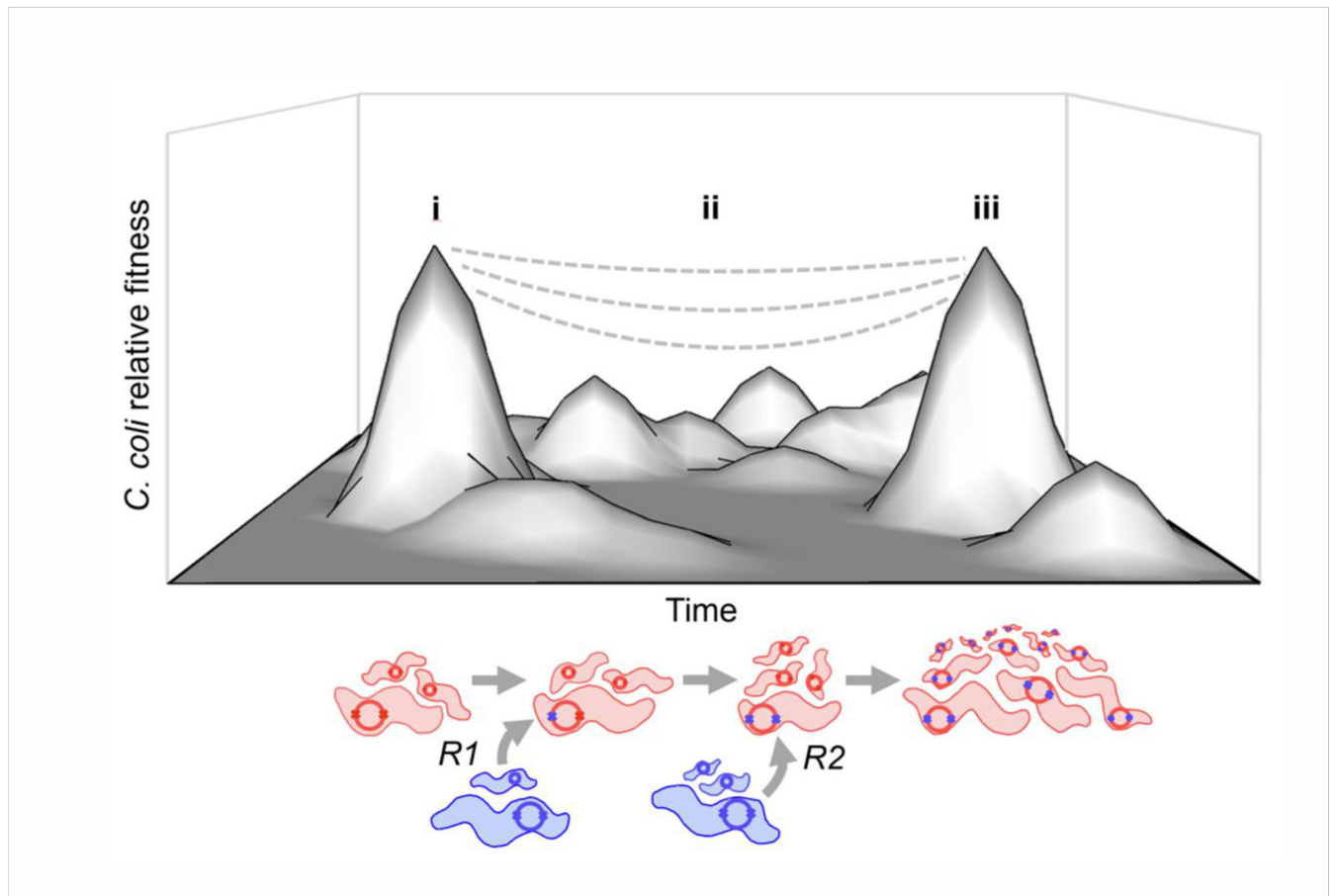


**FIG 5** A two-hit model for core genome recombination in natural *C. coli* populations. Synthetic schematic of a fitness landscape upon which (i) unintrogressed *C. coli* (red) and *C. jejuni* (blue) co-exist. Their genomes (internal circles) harbor haplotype pairs (X-X) that segregate by species. (ii) In a potentially reversible process, horizontal gene transfer occurs (R1) disrupting co-varying genetic elements and reducing the relative fitness of introgressed *C. coli* to varying degrees, and few strains retain mixed *C. coli*-*C. jejuni* haplotypes. (iii) HGT continues (R2) and, where recombined mixed haplotypes survived, ancestral *C. jejuni* haplotype pairs are reinstated in introgressed *C. coli*—some of which outcompete unintrogressed strains. This process potentially provides a means for beneficial adaptations to occur in niche transitions.

## MATERIALS AND METHODS

### Isolates, genome sequencing, and assembly

A total of 973 isolates were used in this study, 827 from *C. coli* and a selection of 146 from a diversity of *C. jejuni* clonal complexes (Data S4). Isolates were sampled mostly in the United Kingdom to maximize environmental and riparian reservoirs and thus the representation of genetic diversity in *C. coli*. Isolates were stored in a 20% (vol/vol) glycerol medium mix at  $-80^{\circ}\text{C}$  and subcultured onto *Campylobacter* selective blood-free agar (mCCDA, CM0739, Oxoid). Plates were incubated at  $42^{\circ}\text{C}$  for 48 hours under microaerobic conditions (5%  $\text{CO}_2$ , 5%  $\text{O}_2$ ), generated using a CampyGen (CN0025, Oxoid) sachet in a sealed container. Subsequent phenotype assays were performed on Brucella agar (CM0271, Oxoid). Colonies were picked onto fresh plates, and genomic DNA extraction was carried out using the QIAamp DNA Mini Kit (QIAGEN; cat. number: 51306) according to the manufacturer's instructions. DNA was eluted in 100–200  $\mu\text{L}$  of the supplied buffer and stored at  $-20^{\circ}\text{C}$ . DNA was quantified using a Nanodrop spectrophotometer, and high-throughput genome sequencing was performed on a MiSeq (Illumina, San Diego, CA, USA), using the Nextera XT Library Preparation Kit with standard protocols involving fragmentation of 2  $\mu\text{g}$  genomic DNA by acoustic shearing to enrich for 600 bp fragments, A-tailing, adapter ligation, and an overlap extension PCR using the Illumina

3 primer set to introduce specific tag sequences between the sequencing and flow cell-binding sites of the Illumina adapter. DNA cleanup was carried out after each step to remove DNA <150 bp using a 1:1 ratio of AMPure paramagnetic beads (Beckman Coulter, Inc., USA). Short-read paired-end data were assembled using the *de novo* assembly algorithm, SPAdes (version 3.10.0) (66). All novel genome sequences ( $n = 475$ ) generated for use in this study are available on NCBI BioProjects [PRJNA689604](#) and [PRJEB11972](#). These were augmented with 498 previously published genomes, and accession numbers for all genomes can be found in Data S4 (16, 26, 41, 52, 67–71).

## Genome archiving, pan-genome content analyses, and phylogenetic reconstruction

Contiguous genome sequence assemblies were individually archived on the web-based database platform PubMLST (72), and sequence type (ST) and clonal complex designation were assigned based upon the *C. jejuni* and *C. coli* multi-locus sequence-typing scheme (73). To examine the full pan-genome content of the data set, a reference pan-genome list was assembled as previously described (34). Briefly, genome assemblies from all 973 genomes in this study were automatically annotated using the RAST/SEED platform (33); the BLAST algorithm was used to determine whether coding sequences from this list were allelic variants of one another or “unique” genes, with two alleles of the same gene being defined as sharing >70% sequence identity on >50% of the sequence length. The prevalence of each gene in the collection of 973 genomes was determined using BLAST with a positive hit in a genome being defined as a local alignment of the reference sequence with the genomic sequence of >70% identity on >50% of the length, as previously described (74). The resulting matrix was analyzed for differentiating core and accessory genome variation. Genes present in all genomes were concatenated to produce a core-genome alignment, used for subsequent phylogenetic reconstructions. Phylogenetic trees were reconstructed using an approximation of maximum-likelihood phylogenetics in FastTree2 (75). This tree was used as an input for ClonalFrameML (40) to produce core genome phylogenies with branch lengths corrected for recombination.

## Inference of introgression

All 973 genomes were aligned to a full reference sequence of *C. coli* strain CVM29710. We conducted imputation for polymorphic sites with missing frequency  $\leq 10\%$  using BEAGLE (76) as previously reported (77). Specifically, haplotype phase (*C. coli* or *C. jejuni*) was inferred for missing markers based on known haplotype data. A total of 286,393 gapless SNPs (~17% of the average *C. coli* genome size) were used for recombination analyses. The co-ancestry of genome-wide haplotype data was inferred based on alignments using chromosome painting and FineStructure (35) as previously described (36). Briefly, ChromoPainter was used to infer chunks of DNA donated from a list of 33 donor groups normalized for sample size to each of 677 ST-CC-828 and 12 CC-1150 recipient haplotypes. Results were summarized into a co-ancestry matrix containing the number of recombination-derived chunks from each donor to each recipient individual. FineStructure was then used for 100,000 iterations of both the burnin and Markov chain Monte Carlo chain to cluster individuals based on the coancestry matrix. The results are visualized as a heat map with each cell indicating the proportion of DNA “chunks” (a series of SNPs with the same expected donor), a recipient receives from each donor.

## Analysis of covariation in bacterial genomes

Non-random allele associations can result from selection and clonal population structure. To control for the latter, our approach identified SNP combinations in independent genetic backgrounds by accounting for the sequence variation associated with the inferred phylogeny (Fig. S6). Based on the alignment of 677 genomes of *C. coli* CC-828, a first phylogenetic tree was created using PhyML (78). ClonalFrameML (40) was

then applied to correct the tree by accounting for the effect of recombination and also to infer the ancestral sequence of each node. Covariance was assessed for pairs of biallelic sites across the genome using a CTMC model as follows. Briefly, let  $A$  and  $a$  denote the two alleles of the first site and  $B$  and  $b$  denote the two alleles of the second site so that there are four states in total for the pair of sites ( $ab$ ,  $Ab$ ,  $aB$ , and  $AB$ ). The four substitution rates from  $A$  to  $a$ , from  $a$  to  $A$ , from  $B$  to  $b$ , and from  $b$  to  $B$  are not assumed to be identical, to allow for differences in substitution rates in different parts of the genome and also to allow for non-equal rates of forward and backward substitution (e.g., as a result of recombination opportunities). Assuming no epistatic effect between the two sites ( $\epsilon = 1$ ), the model  $M_0$  has four free parameters ( $\alpha_1$ ,  $\alpha_2$ ,  $\beta_1$ , and  $\beta_2$ ) representing independent substitutions at the two sites. We expand model  $M_0$  with an additional fifth parameter  $\epsilon > 1$  into model  $M_1$  which is such that the state  $AB$  where the first site is allele  $A$  and the second site is allele  $B$  is favored relative to the other three sites  $ab$ ,  $aB$ , and  $Ab$ . Specifically, the state  $AB$  has a probability increased by a factor  $\epsilon^2$  in the stationary distribution of the CTMC of model  $M_1$  compared to model  $M_0$ .

Both models  $M_0$  (with four parameters) and  $M_1$  (with five parameters) are fitted to the data using maximum likelihood techniques, where the likelihood is equal to the product for every branch of the tree of the state at the bottom of the branch given the state at the top. The two fitted models  $M_0$  and  $M_1$  are then compared using a likelihood-ratio test (LRT) as follows: since  $M_0$  is nested with  $M_1$ , two times their difference in log-likelihood is expected to be distributed according to a chi-square distribution with the number of degrees of freedom equal to the difference in their dimensionality, which is 1. This LRT returns a  $P$ -value for the significance of a covariation effect, and a Bonferroni correction is applied to determine a conservative cutoff of significance that accounts for multiple testing. Furthermore, the test is applied only to pairs of sites separated by  $>20$  kbp to reduce the chance that they were the result of a single recombination event, consistent with estimates of the length of recombined DNA sequence in quantitative bacterial transformation experiments (49, 79) and evidence from *Campylobacter* genome analyses that show that LD for pairs of sites decreases with distance to approximately 5 kbp and then remains at the same level for very distant sites (Fig. 3B) (52). It is still possible, of course, that rare recombination events would stretch 20 kbp (49–51), but for this to have an effect on the analysis of epistasis, it would have to have happened several times for the same pairs of sites against different genomic backgrounds, which become quite unlikely just by chance. This phylogenetically aware approach to testing for covariance presents the advantage to naturally account for both population structure and the effect of recombination (80). The script implementing this coevolution test is available in R at <https://github.com/xavierdidelot/campy>.

## Quantifying covariation between recombined and unrecombined genomic regions

The results of the introgression and covariation analyses were combined so that for each pair of significantly covarying SNPs ( $P$ -value  $< 10^{-8}$ ), haplotype frequency was calculated among the 689 recipient-introgressed *C. coli* clade-1 strains as well as among the donor *C. coli* (ancestral) and *C. jejuni* strains, respectively. If the most frequent haplotype of the pair is the same between the donor *C. coli* (ancestral) and *C. jejuni*, it was classified as “no polymorphism.” Otherwise, if the most frequent haplotype accounted for  $>90\%$  among the recipients, it was classified as either “*C. jejuni* ( $>90\%$ )” or “*C. coli* ( $>90\%$ )” if it was the same as that of donor *C. jejuni* or *C. coli* (ancestral) (inset in Fig. 2C). If the most frequent haplotype accounted for  $\leq 90\%$  among the recipients, the top two most frequent haplotypes (written as major and minor haplotypes in this manuscript) were indicated as either “*C. jejuni/C. coli*,” “*C. jejuni/other*,” “*C. coli/C. jejuni*,” “*C. coli/other*,” “*other/C. coli*,” “*other/C. jejuni*,” and “*other/other*,” and the frequency of the major and minor haplotypes was calculated. For example, where the haplotype frequencies were as follows, AA = 285, TA = 192, TG = 181, AG = 27, A- = 2, -- = 1, -A = 1, AA is the major haplotype, frequency of which is 41.3%. To visualize linkage disequilibrium decay across

the genome, 689 introgressed *C. coli* isolate genomes (ST-828 and ST-1150 complex, Data S4) were aligned to the *C. coli* CVM29710 reference genome, and variant calling was conducted on SAM files, using a combination of Samtools and Bcftools version 1.14 (81, 82). LD was determined using PLINK version 1.90b7.2 (83), using R2 as statistical criterion. For simplification, LD was calculated as the average value within 100-bp blocks visualized as a function of genomic distance. The maximum LD was determined for 12 epistatic positions of interest (Fig. 3B).

### Mutagenesis and complementation cloning

Genes *cj1167*, *cj1168c* (here designated *self* for selenium transport for formate dehydrogenase), *cj1171c* (*ppi*), *cj1507c* (*modE*), *cj1508c* (*fdhD*), and *cj1500* (*fdhT*) were deleted by gene replacement mutagenesis, with the majority of the open reading frame replaced by an antibiotic resistance cassette. Mutagenesis plasmids were generated by the isothermal assembly method using the HiFi system (NEB, UK). In brief, flanking regions of target genes were PCR amplified from genomic DNA using primers with adaptors homologous to either the backbone vector pGEM3ZF or the antibiotic resistance cassette (Data S5). pGEM3ZF was linearized by digestion with HincII. The kanamycin and chloramphenicol resistance cassettes were PCR amplified from pJMK30 and pAV35, respectively (84). Four fragments consisting of linearized pGEM3ZF, antibiotic resistance cassette, and two flanking regions were combined in equimolar amounts and mixed with 2× HiFi reagent (NEB, UK) and incubated at 50°C for 1 hour. The fragments combine such that the gene fragments flank the antibiotic resistance cassette, in the same transcriptional orientation, within the vector. Mutagenesis plasmids were transformed into *C. jejuni* NCTC 11168 by electroporation. Spontaneous double-crossover recombinants were selected for using the appropriate antibiotic and correct insertion into the target gene confirmed by PCR screening. For genetic complementation of mutants, genes *cj1168c* (*self*), *cj1507c* (*modE*), *cj1508c* (*fdhD*), and *cj1500* (*fdhT*) were PCR amplified from genomic DNA, restriction digested with MfeI and XbaI, then ligated into similarly digested pRRA (85) (Data S5). The orientation of insertion allowed the target gene to be expressed constitutively by a chloramphenicol resistance gene-derived promoter within the vector. Complementation plasmids were transformed into *C. jejuni* by electroporation. Spontaneous double-crossover recombinants were selected using apramycin, and correct insertion into the ribosomal locus was confirmed by PCR screening.

### Growth of *C. jejuni*

Microaerobic growth cabinets (Don Whitley, UK) were maintained at 42°C with an atmosphere of 10% O<sub>2</sub>, 5% CO<sub>2</sub>, and 85% N<sub>2</sub> (vol/vol). *C. jejuni* was grown on Columbia base agar containing 5% (vol/vol) defibrinated horse blood. Selective antibiotics were added to plates as appropriate at the following concentrations: 50 µg mL<sup>-1</sup> kanamycin, 20 µg mL<sup>-1</sup> chloramphenicol, and 60 µg mL<sup>-1</sup> apramycin. Muller-Hinton broth supplemented with 20 mM L-serine was used as a rich medium. Minimal medium was prepared from a supplied MEM base (51200–38, Thermo Scientific, UK) with the following additions: 20 mM L-serine, 0.5 mM sodium pyruvate, 50 µM sodium metabisulfite, 4 mM L-cysteine, HCl, 2 mM L-methionine, 5 mM L-glutamine, 50 µM ferrous sulfate, 100 µM ascorbic acid, 1 µM vitamin B12, 5 µM sodium molybdate, and 1 µM sodium tungstate. Selenium was then added as appropriate from stocks of sodium selenate or sodium selenite prepared in dH<sub>2</sub>O. For assays, cells were washed and suspended in sterile phosphate-buffered saline (PBS, Sigma-Aldrich).

### Respiration rates with formate

Cells were first grown in MH broth for 12 hours, then washed thoroughly in PBS before inoculating minimal media without an added selenium source. The appropriate concentrations were determined by serial dilution trials, and it was subsequently found that *C. jejuni* has a strong preference for selenite over selenate, as equivalent FDH activity

requires some 1,000-fold greater concentration of selenate than selenite (Fig. S9). These cultures were grown for 8 hours before the cells were thoroughly washed again, then used to inoculate further minimal media, with a selenium source added as appropriate, and grown for 10 hours. This passaging was necessary to remove all traces of selenium from the inoculum, such that control cultures without selenium added had negligible (FDH) activity. Assay cultures were again thoroughly washed before the equivalent of 20 mL at an optical density of 0.8 at 600 nm was finally suspended in 1 mL of PBS. Formate-dependent oxygen consumption by whole cells was measured in a Clark-type electrode using 20 mM sodium formate as electron donor. The electrode was calibrated with air-saturated PBS assuming 220 nmol dissolved O<sub>2</sub> per milliliter at 37°C. In the electrode, 200 µL of the dense cell suspension was added to 800 µL air-saturated PBS for a final volume of 1 mL. The chamber was sealed, and the suspension was allowed to equilibrate for 2 minutes. The assay was initiated by the addition of 20 µL of 1 M sodium formate (prepared in PBS), and the rate of oxygen consumption recorded for 90 s. The total protein concentration of the cell suspensions was determined by Lowry assay, and the specific rate of formate-dependent oxygen consumption expressed as nanomolar oxygen consumed per minute per milligram total protein.

### ACKNOWLEDGMENTS

Funding for this work came from Wellcome Trust grant 088786/C/09/Z (S.K.S.), Medical Research Council (MRC) grant MR/M501608/1 (S.K.S.), Medical Research Council (MRC) grant MR/L015080/1 (S.K.S.), Food Standards Agency project FS101087 (S.K.S.), and Biotechnology & Biological Sciences Research Council (BBSRC) grant BB/S014497/1 (D.J.K.).

Conceptualization and study design: S.K.S., X.D., D.F., K.Y., D.J.K., A.J.T., P.K. Sample collection: S.K.S., A.H.M.V.V., N.J.W. Laboratory work: A.J.T., L.M., M.D.H., B.P. Data archiving: B.P., K.A.J. Data analysis: A.J.T., X.D., K.Y., L.M., J.K.C., E.M., S.P., S.B., S.K.S., J.C., S.K. Data interpretation: K.Y., X.D., S.K.S., M.C.J.M., J.P., D.J.K., A.J.T., D.F., P.K. Writing: S.K.S., C.M.K., A.J.T., D.J.K., P.K.

### AUTHOR AFFILIATIONS

<sup>1</sup>School of Biological Sciences, University of Reading, Reading, United Kingdom

<sup>2</sup>Antimicrobial Resistance Research Center, National Institute of Infectious Diseases, Tokyo, Japan

<sup>3</sup>Department of Biology, University of Oxford, Oxford, United Kingdom

<sup>4</sup>Swansea University Medical School, Institute of Life Science, Swansea, United Kingdom

<sup>5</sup>The Department of Biology and Biochemistry, University of Bath, Bath, United Kingdom

<sup>6</sup>Oslo Centre for Biostatistics and Epidemiology, Oslo University Hospital, Oslo, Norway

<sup>7</sup>Department of Mathematics and Statistics, Helsinki Institute for Information Technology, University of Helsinki, Helsinki, Finland

<sup>8</sup>Sir William Dunn School of Pathology, University of Oxford, Oxford, United Kingdom

<sup>9</sup>Bristol Veterinary School, University of Bristol, Bristol, United Kingdom

<sup>10</sup>Department of Epidemiology and Population Health, Institute of Infection and Global Health, University of Liverpool, Leahurst Campus, Wirral, United Kingdom

<sup>11</sup>School of Veterinary Medicine, University of Surrey, Guildford, United Kingdom

<sup>12</sup>Department of Veterinary Medicine, University of Cambridge, Cambridge, United Kingdom

<sup>13</sup>Parasites and Microbes, Wellcome Sanger Institute, Cambridge, United Kingdom

<sup>14</sup>The Centre for Microbes, Development and Health, Institut Pasteur of Shanghai, Shanghai, China

<sup>15</sup>The Pathogen and Microbiome Institute, Northern Arizona University, Flagstaff, Arizona, USA

<sup>16</sup>Department of Biological Sciences, Northern Arizona University, Flagstaff, Arizona, USA

<sup>17</sup>Department of Statistics, School of Life Sciences, University of Warwick, Coventry, United Kingdom

<sup>18</sup>School of Biosciences, University of Sheffield, Sheffield, United Kingdom

### AUTHOR ORCID*s*

Aidan J. Taylor  <http://orcid.org/0000-0003-1006-1205>  
Ben Pascoe  <https://orcid.org/0000-0001-6376-5121>  
Arnoud H. M. van Vliet  <http://orcid.org/0000-0003-0203-1305>  
Julian Parkhill  <https://orcid.org/0000-0002-7069-5958>  
Martin C. J. Maiden  <http://orcid.org/0000-0001-6321-5138>  
Daniel Falush  <https://orcid.org/0000-0002-2956-0795>  
Paul Keim  <http://orcid.org/0000-0003-0089-5820>  
David J. Kelly  <http://orcid.org/0000-0002-0770-6845>  
Samuel K. Sheppard  <http://orcid.org/0000-0001-6901-3203>

### FUNDING

Funder	Grant(s)	Author(s)
<a href="#">Wellcome Trust (WT)</a>	088786/C/09/Z	Samuel K. Sheppard
<a href="#">UKRI   Medical Research Council (MRC)</a>	MR/M501608/1	Samuel K. Sheppard
<a href="#">UKRI   Medical Research Council (MRC)</a>	MR/L015080/1	Samuel K. Sheppard
<a href="#">Food Standards Agency (FSA)</a>	FS101087	Samuel K. Sheppard
<a href="#">UKRI   Biotechnology and Biological Sciences Research Council (BBSRC)</a>	BB/S014497/1	David J. Kelly
<a href="#">Cowden Endowment for Food Microbiology</a>	2022/23	Paul Keim

### DIRECT CONTRIBUTION

This article is a direct contribution from Paul Keim, a Fellow of the American Academy of Microbiology, who arranged for and secured reviews by Timothy D. Read, Emory University School of Medicine, and David S. Guttman, University of Toronto.

### DATA AVAILABILITY

Short-read sequence data for all isolates sequenced in this study are deposited in the sequence read archive (SRA) and can be found associated with NCBI BioProjects [PRJNA689604](#) and [PRJEB11972](#). These were augmented with 498 previously published genomes, and assembled genomes are available on Figshare ([doi.org/10.6084/m9.figshare.13521683](https://doi.org/10.6084/m9.figshare.13521683)). Accession numbers for all genomes are included in Data S4. Source data are provided for this paper (Data S2).

### ADDITIONAL FILES

The following material is available [online](#).

#### Supplemental Material

**Data S1** (mBio00581-24-S0001.xlsx). Maximum SNP frequency and covarying *P*-values per gene.

**Data S2** (mBio00581-24-S0002.xlsx). Source data.

**Data S3** (mBio00581-24-S0003.xlsx). Genes with covarying SNPs identified in this study.

**Data S4** (mBio00581-24-S0004.xlsx). Isolates and genomes used in this study.

**Data S5** (mBio00581-24-S0005.xlsx). Primers used in this study.

**Supplemental Figures** (mBio00581-24-S0006.pdf). Figures S1 to S8.



## REFERENCES

- Ochman H, Lawrence JG, Groisman EA. 2000. Lateral gene transfer and the nature of bacterial innovation. *Nature* 405:299–304. <https://doi.org/10.1038/35012500>
- Koonin EV, Makarova KS, Aravind L. 2001. Horizontal gene transfer in prokaryotes: quantification and classification. *Annu Rev Microbiol* 55:709–742. <https://doi.org/10.1146/annurev.micro.55.1.709>
- HALDANE JB. 1964. A defense of beanbag genetics. *Perspect Biol Med* 7:343–359. <https://doi.org/10.1353/pbm.1964.0042>
- Bateson W. 2009. Darwin and modern science, p 85–101. In Seward AC (ed), *Heredity and variation in modern lights*. Cambridge University Press, Cambridge.
- Fisher RA. 1919. The correlation between relatives on the supposition of Mendelian inheritance. *Trans R Soc Edinb* 52:399–433. <https://doi.org/10.1017/S0080456800012163>
- Wright S. 1931. Evolution in Mendelian populations. *Genetics* 16:97–159. <https://doi.org/10.1093/genetics/16.2.97>
- Dobzhansky T. 1936. Studies on hybrid sterility. II. localization of sterility factors in *Drosophila pseudoobscura* hybrids. *Genetics* 21:113–135. <https://doi.org/10.1093/genetics/21.2.113>
- Dobzhansky T. 1937. *Genetics and the origin of species*. Columbia University Press, New York.
- Muller HJ. 1940. Bearings of the 'Drosophila' work on systematics. *The New Systematics* 1940:185–268.
- Muller HJ. 1942. Isolating mechanisms, evolution, and temperature. *Biology Symposium* 6:71–125.
- Kimura M. 1965. Attainment of quasi linkage equilibrium when gene frequencies are changing by natural selection. *Genetics* 52:875–890. <https://doi.org/10.1093/genetics/52.5.875>
- Neher RA, Shraiman BI. 2009. Competition between recombination and epistasis can cause a transition from allele to genotype selection. *Proc Natl Acad Sci U S A* 106:6866–6871. <https://doi.org/10.1073/pnas.0812560106>
- Wilson DJ, Gabriel E, Leatherbarrow AJH, Cheesbrough J, Gee S, Bolton E, Fox A, Hart CA, Diggle PJ, Fearnhead P. 2009. Rapid evolution and the importance of recombination to the gastroenteric pathogen *Campylobacter jejuni*. *Mol Biol Evol* 26:385–397. <https://doi.org/10.1093/molbev/msn264>
- Gibson B, Wilson DJ, Feil E, Eyre-Walker A. 2018. The distribution of bacterial doubling times in the wild. *Proc Biol Sci* 285:285. <https://doi.org/10.1098/rspb.2018.0789>
- Vos M, Didelot X. 2009. A comparison of homologous recombination rates in bacteria and archaea. *ISME J* 3:199–208. <https://doi.org/10.1038/ismej.2008.93>
- Calland JK, Pascoe B, Bayliss SC, Mourkas E, Berthenet E, Thorpe HA, Hitchings MD, Feil EJ, Corander J, Blaser MJ, Falush D, Sheppard SK. 2021. Quantifying bacterial evolution in the wild: a birthday problem for campylobacter lineages. *PLoS Genet* 17:e1009829. <https://doi.org/10.1371/journal.pgen.1009829>
- Arnold BJ, Gutmann MU, Grad YH, Sheppard SK, Corander J, Lipsitch M, Hanage WP. 2018. Weak epistasis may drive adaptation in recombining bacteria. *Genetics* 208:1247–1260. <https://doi.org/10.1534/genetics.117.300662>
- Sheppard SK, Guttman DS, Fitzgerald JR. 2018. Population genomics of bacterial host adaptation. *Nat Rev Genet* 19:549–565. <https://doi.org/10.1038/s41576-018-0032-z>
- Andreani NA, Hesse E, Vos M. 2017. Prokaryote genome fluidity is dependent on effective population size. *ISME J* 11:1719–1721. <https://doi.org/10.1038/ismej.2017.36>
- Vos M, Eyre-Walker A. 2017. Are pangenomes adaptive or not? *Nat Microbiol* 2:1576. <https://doi.org/10.1038/s41564-017-0067-5>
- Shapiro BJ. 2017. The population genetics of pangenomes. *Nat Microbiol* 2:1574. <https://doi.org/10.1038/s41564-017-0066-6>
- McInerney JO, McNally A, O'Connell MJ. 2017. Why prokaryotes have pangenomes. *Nat Microbiol* 2:17040. <https://doi.org/10.1038/nmicrobiol.2017.40>
- Orr HA. 1996. Dobzhansky, Bateson, and the genetics of speciation. *Genetics* 144:1331–1335. <https://doi.org/10.1093/genetics/144.4.1331>
- Fraser C, Hanage WP, Spratt BG. 2007. Recombination and the nature of bacterial speciation. *Science* 315:476–480. <https://doi.org/10.1126/science.1127573>
- Sheppard SK, McCarthy ND, Falush D, Maiden MCJ. 2008. Convergence of *Campylobacter* species: implications for bacterial evolution. *Science* 320:237–239. <https://doi.org/10.1126/science.1155532>
- Sheppard SK, Didelot X, Jolley KA, Darling AE, Pascoe B, Meric G, Kelly DJ, Cody A, Colles FM, Strachan NJC, Ogden ID, Forbes K, French NP, Carter P, Miller WG, McCarthy ND, Owen R, Litrup E, Egholm M, Affourtit JP, Bentley SD, Parkhill J, Maiden MCJ, Falush D. 2013. Progressive genome-wide Introgression in agricultural *Campylobacter coli*. *Mol Ecol* 22:1051–1064. <https://doi.org/10.1111/mec.12162>
- Smith JT, Andam CP. 2021. Extensive horizontal gene transfer within and between species of coagulase-negative staphylococcus. *Genome Biol Evol* 13:evab206. <https://doi.org/10.1093/gbe/evab206>
- Lee IPA, Andam CP. 2022. Frequencies and characteristics of genome-wide recombination in *Streptococcus agalactiae*, *Streptococcus pyogenes*, and *Streptococcus suis*. *Sci Rep* 12:1515. <https://doi.org/10.1038/s41598-022-04995-5>
- Méric G, Miragaia M, de Been M, Yahara K, Pascoe B, Mageiros L, Mikhail J, Harris LG, Wilkinson TS, Rolo J, Lambie S, Bray JE, Jolley KA, Hanage WP, Bowden R, Maiden MCJ, Mack D, de Lencastre H, Feil EJ, Corander J, Sheppard SK. 2015. Ecological overlap and horizontal gene transfer in *Staphylococcus aureus* and *Staphylococcus epidermidis*. *Genome Biol Evol* 7:1313–1328. <https://doi.org/10.1093/gbe/evw066>
- Sheppard SK, Dallas JF, Strachan NJC, MacRae M, McCarthy ND, Wilson DJ, Gormley FJ, Falush D, Ogden ID, Maiden MCJ, Forbes KJ. 2009. *Campylobacter* genotyping to determine the source of human infection. *Clin Infect Dis* 48:1072–1078. <https://doi.org/10.1086/597402>
- Sheppard SK, Maiden MCJ. 2015. The evolution of *Campylobacter jejuni* and *Campylobacter coli*. *Cold Spring Harb Perspect Biol* 7:a018119. <https://doi.org/10.1101/cshperspect.a018119>
- Knudson AG. 1971. Mutation and cancer: statistical study of retinoblastoma. *Proc Natl Acad Sci U S A* 68:820–823. <https://doi.org/10.1073/pnas.68.4.820>
- Aziz RK, Bartels D, Best AA, DeJongh M, Disz T, Edwards RA, Formsma K, Gerdes S, Glass EM, Kubal M, et al. 2008. The RAST server: rapid annotations using subsystems technology. *BMC Genomics* 9:75. <https://doi.org/10.1186/1471-2164-9-75>
- Méric G, Yahara K, Mageiros L, Pascoe B, Maiden MCJ, Jolley KA, Sheppard SK. 2014. A reference pan-genome approach to comparative bacterial genomics: identification of novel epidemiological markers in pathogenic *Campylobacter*. *PLOS One* 9:e92798. <https://doi.org/10.1371/journal.pone.0092798>
- Lawson DJ, Hellenthal G, Myers S, Falush D. 2012. Inference of population structure using dense haplotype data. *PLoS Genet* 8:e1002453. <https://doi.org/10.1371/journal.pgen.1002453>
- Yahara K, Didelot X, Ansari MA, Sheppard SK, Falush D. 2014. Efficient inference of recombination hot regions in bacterial genomes. *Mol Biol Evol* 31:1593–1605. <https://doi.org/10.1093/molbev/msu082>
- Cohan FM. 2002. Sexual isolation and speciation in bacteria, p 359–370. In *Genetics of mate choice: from sexual selection to sexual isolation*. Springer.
- Ansari MA, Didelot X. 2014. Inference of the properties of the recombination process from whole bacterial genomes. *Genetics* 196:253–265. <https://doi.org/10.1534/genetics.113.157172>
- Retchless AC, Lawrence JG. 2010. Phylogenetic incongruence arising from fragmented speciation in enteric bacteria. *Proc Natl Acad Sci U S A* 107:11453–11458. <https://doi.org/10.1073/pnas.1001291107>
- Didelot X, Wilson DJ. 2015. ClonalFrameML: efficient inference of recombination in whole bacterial genomes. *PLoS Comput Biol* 11:e1004041. <https://doi.org/10.1371/journal.pcbi.1004041>
- Dearlove BL, Cody AJ, Pascoe B, Méric G, Wilson DJ, Sheppard SK. 2016. Rapid host switching in generalist *Campylobacter* strains erodes the signal for tracing human infections. *ISME J* 10:721–729. <https://doi.org/10.1038/ismej.2015.149>
- Weerakoon DR, Borden NJ, Goodson CM, Grimes J, Olson JW. 2009. The role of respiratory donor enzymes in *Campylobacter jejuni* host

- colonization and physiology. *Microb Pathog* 47:8–15. <https://doi.org/10.1016/j.micpath.2009.04.009>
43. Taylor AJ, Kelly DJ. 2019. The function, biogenesis and regulation of the electron transport chains in *Campylobacter jejuni*: new insights into the bioenergetics of a major food-borne pathogen. *Adv Microb Physiol* 74:239–329. <https://doi.org/10.1016/bs.ampbs.2019.02.003>
  44. Smart JP, Cliff MJ, Kelly DJ. 2009. A role for tungsten in the biology of *Campylobacter jejuni*: tungstate stimulates formate dehydrogenase activity and is transported via an ultra-high affinity ABC system distinct from the molybdate transporter. *Mol Microbiol* 74:742–757. <https://doi.org/10.1111/j.1365-2958.2009.06902.x>
  45. Doerler WT, Sikdar R, Kumar S, Boughner LA. 2013. New functions for the ancient DedA membrane protein family. *J Bacteriol* 195:3–11. <https://doi.org/10.1128/JB.01006-12>
  46. Ledgham F, Quest B, Vallaes T, Mergeay M, Covès J. 2005. A probable link between the DedA protein and resistance to selenite. *Res Microbiol* 156:367–374. <https://doi.org/10.1016/j.resmic.2004.11.003>
  47. Shaw FL, Mulholland F, Le Gall G, Porcelli I, Hart DJ, Pearson BM, van Vliet AHM. 2012. Selenium-dependent biogenesis of formate dehydrogenase in *Campylobacter jejuni* is controlled by the *fdhTU* accessory genes. *J Bacteriol* 194:3814–3823. <https://doi.org/10.1128/JB.06586-11>
  48. Sheppard SK, McCarthy ND, Jolley KA, Maiden MCJ. 2011. Introgression in the genus *Campylobacter*: generation and spread of mosaic alleles. *Microbiology* 157:1066–1074. <https://doi.org/10.1099/mic.0.045153-0>
  49. Croucher NJ, Harris SR, Barquist L, Parkhill J, Bentley SD. 2012. A high-resolution view of genome-wide pneumococcal transformation. *PLoS Pathog* 8:e1002745. <https://doi.org/10.1371/journal.ppat.1002745>
  50. He M, Sebaihia M, Lawley TD, Stabler RA, Dawson LF, Martin MJ, Holt KE, Seth-Smith HMB, Quail MA, Rance R, Brooks K, Churcher C, Harris D, Bentley SD, Burrows C, Clark L, Corton C, Murray V, Rose G, Thurston S, van Tonder A, Walker D, Wren BW, Dougan G, Parkhill J. 2010. Evolutionary dynamics of *Clostridium difficile* over short and long time scales. *Proc Natl Acad Sci U S A* 107:7527–7532. <https://doi.org/10.1073/pnas.0914322107>
  51. Power PM, Bentley SD, Parkhill J, Moxon ER, Hood DW. 2012. Investigations into genome diversity of *Haemophilus influenzae* using whole genome sequencing of clinical isolates and laboratory transformants. *BMC Microbiol* 12:273. <https://doi.org/10.1186/1471-2180-12-273>
  52. Yahara K, Méric G, Taylor AJ, de Vries SPW, Murray S, Pascoe B, Mageiros L, Torralbo A, Vidal A, Ridley A, et al. 2017. Genome-wide association of functional traits linked with *Campylobacter jejuni* survival from farm to fork. *Environ Microbiol* 19:361–380. <https://doi.org/10.1111/1462-2920.13628>
  53. Arnoux P, Ruppelt C, Oudouhou F, Lavergne J, Siponen MI, Toci R, Mendel RR, Bittner F, Pignol D, Magalon A, Walburger A. 2015. Sulphur shuttling across a chaperone during molybdenum cofactor maturation. *Nat Commun* 6:6148. <https://doi.org/10.1038/ncomms7148>
  54. Taveirne ME, Sikes ML, Olson JW. 2009. Molybdenum and tungsten in *Campylobacter jejuni*: Their physiological role and identification of separate transporters regulated by a single ModE-like protein. *Mol Microbiol* 74:758–771. <https://doi.org/10.1111/j.1365-2958.2009.06901.x>
  55. Aguilar-Barajas E, Díaz-Pérez C, Ramírez-Díaz MI, Riveros-Rosas H, Cervantes C. 2011. Bacterial transport of sulfate, molybdate, and related oxyanions. *Biomaterials* 24:687–707. <https://doi.org/10.1007/s10534-011-9421-x>
  56. Markovic R, Ciric J, Drljacic A, Šefer D, Jovanovic I, Jovanovic D, Milanovic S, Trbovic D, Radulovic S, Baltic MŽ, Starcevic M. 2018. The effects of dietary selenium-yeast level on glutathione peroxidase activity, tissue selenium content, growth performance, and carcass and meat quality of broilers. *Poult Sci* 97:2861–2870. <https://doi.org/10.3382/ps/pey117>
  57. Choct M, Naylor AJ, Reinke N. 2004. Selenium supplementation affects broiler growth performance, meat yield and feather coverage. *Br Poult Sci* 45:677–683. <https://doi.org/10.1080/00071660400006495>
  58. Cemin HS, Vieira SL, Stefanello C, Kindlein L, Ferreira TZ, Fireman AK. 2018. Broiler responses to increasing selenium supplementation using Zn-L-selenomethionine with special attention to breast myopathies. *Poult Sci* 97:1832–1840. <https://doi.org/10.3382/ps/pey001>
  59. National Research Council. 1994. Nutrient requirements of poultry. Vol. 155 p. National Academy Press, Washington D.C.
  60. Jensen LS, Colnago GL, Takahashi K, Akiba Y. 1986. Dietary selenium status and plasma thyroid hormones in chicks. *Biol Trace Elem Res* 10:11–18. <https://doi.org/10.1007/BF02795314>
  61. Thomas MT, Shepherd M, Poole RK, van Vliet AHM, Kelly DJ, Pearson BM. 2011. Two respiratory enzyme systems in *Campylobacter jejuni* NCTC 11168 contribute to growth on l-lactate. *Environ Microbiol* 13:48–61. <https://doi.org/10.1111/j.1462-2920.2010.02307.x>
  62. Ünal CM, Steinert M. 2014. Microbial peptidyl-prolyl cis/trans isomerases (PPIases): virulence factors and potential alternative drug targets. *Microbiol Mol Biol Rev* 78:544–571. <https://doi.org/10.1128/MMBR.00015-14>
  63. Oren Y, Smith MB, Johns NI, Kaplan Zeevi M, Biran D, Ron EZ, Corander J, Wang HH, Alm EJ, Pupko T. 2014. Transfer of noncoding DNA drives regulatory rewiring in bacteria. *Proc Natl Acad Sci U S A* 111:16112–16117. <https://doi.org/10.1073/pnas.1413272111>
  64. Arnold B, Sohail M, Wadsworth C, Corander J, Hanage WP, Sunyaev S, Grad YH. 2020. Fine-scale haplotype structure reveals strong signatures of positive selection in a recombining bacterial pathogen. *Mol Biol Evol* 37:417–428. <https://doi.org/10.1093/molbev/msz225>
  65. Wadsworth CB, Arnold BJ, Sater MRA, Grad YH. 2018. Azithromycin resistance through interspecific acquisition of an epistasis-dependent efflux pump component and transcriptional regulator in *Neisseria gonorrhoeae*. *mBio* 9:e01419-18. <https://doi.org/10.1128/mBio.01419-18>
  66. Bankevich A, Nurk S, Antipov D, Gurevich AA, Dvorkin M, Kulikov AS, Lesin VM, Nikolenko SI, Pham S, Pribelski AD, Pyshkin AV, Sirotkin AV, Vyahhi N, Tesler G, Alekseyev MA, Pevzner PA. 2012. SPAdes: a new genome assembly algorithm and its applications to single-cell sequencing. *J Comput Biol* 19:455–477. <https://doi.org/10.1089/cmb.2012.0021>
  67. Sheppard SK, Didelot X, Méric G, Torralbo A, Jolley KA, Kelly DJ, Bentley SD, Maiden MCJ, Parkhill J, Falush D. 2013. Genome-wide association study identifies vitamin B5 biosynthesis as a host specificity factor in *Campylobacter*. *Proc Natl Acad Sci U S A* 110:11923–11927. <https://doi.org/10.1073/pnas.1305591110>
  68. Sheppard Samuel K, Cheng L, Méric G, de Haan CPA, Llerena A-K, Marttinen P, Vidal A, Ridley A, Clifton-Hadley F, Connor TR, Strachan NJC, Forbes K, Colles FM, Jolley KA, Bentley SD, Maiden MCJ, Hänninen M-L, Parkhill J, Hanage WP, Corander J. 2014. Cryptic ecology among host generalist *Campylobacter jejuni* in domestic animals. *Mol Ecol* 23:2442–2451. <https://doi.org/10.1111/mec.12742>
  69. Pascoe B, Méric G, Yahara K, Wimalaratna H, Murray S, Hitchings MD, Sproston EL, Carrillo CD, Taboada EN, Cooper KK, Huynh S, Cody AJ, Jolley KA, Maiden MCJ, McCarthy ND, Didelot X, Parker CT, Sheppard SK. 2017. Local genes for local bacteria: evidence of allopatry in the genomes of transatlantic *Campylobacter* populations. *Mol Ecol* 26:4497–4508. <https://doi.org/10.1111/mec.14176>
  70. Pascoe B, Schiaffino F, Murray S, Méric G, Bayliss SC, Hitchings MD, Mourkas E, Calland JK, Burga R, Yori PP, Jolley KA, Cooper KK, Parker CT, Olortegui MP, Kosek MN, Sheppard SK. 2020. Genomic epidemiology of *Campylobacter jejuni* associated with asymptomatic pediatric infection in the Peruvian Amazon. *PLoS Negl Trop Dis* 14:e0008533. <https://doi.org/10.1371/journal.pntd.0008533>
  71. Mourkas E, Taylor AJ, Méric G, Bayliss SC, Pascoe B, Mageiros L, Calland JK, Hitchings MD, Ridley A, Vidal A, Forbes KJ, Strachan NJC, Parker CT, Parkhill J, Jolley KA, Cody AJ, Maiden MCJ, Kelly DJ, Sheppard SK. 2020. Agricultural intensification and the evolution of host specialism in the enteric pathogen *Campylobacter jejuni*. *Proc Natl Acad Sci U S A* 117:11018–11028. <https://doi.org/10.1073/pnas.1917168117>
  72. Jolley KA, Maiden MCJ. 2010. BIGSdb: scalable analysis of bacterial genome variation at the population level. *BMC Bioinformatics* 11:595. <https://doi.org/10.1186/1471-2105-11-595>
  73. Dingle KE, Colles FM, Wareing DR, Ure R, Fox AJ, Bolton FE, Bootsma HJ, Willems RJ, Urwin R, Maiden MC. 2001. Multilocus sequence typing system for *Campylobacter jejuni*. *J Clin Microbiol* 39:14–23. <https://doi.org/10.1128/JCM.39.1.14-23.2001>
  74. Sheppard SK, Jolley KA, Maiden MCJ. 2012. A gene-by-gene approach to bacterial population genomics: whole genome MLST of *Campylobacter*. *Genes (Basel)* 3:261–277. <https://doi.org/10.3390/genes3020261>
  75. Price MN, Dehal PS, Arkin AP. 2010. FastTree 2 – approximately maximum-likelihood trees for large alignments. *PLoS One* 5:e9490. <https://doi.org/10.1371/journal.pone.0009490>

76. Browning BL, Browning SR. 2009. A unified approach to genotype imputation and haplotype-phase inference for large data sets of trios and unrelated individuals. *Am J Hum Genet* 84:210–223. <https://doi.org/10.1016/j.ajhg.2009.01.005>
77. Yahara K, Furuta Y, Oshima K, Yoshida M, Azuma T, Hattori M, Uchiyama I, Kobayashi I. 2013. Chromosome painting *in Silico* in a bacterial species reveals fine population structure. *Mol Biol Evol* 30:1454–1464. <https://doi.org/10.1093/molbev/mst055>
78. Guindon S, Dufayard J-F, Lefort V, Anisimova M, Hordijk W, Gascuel O. 2010. New algorithms and methods to estimate maximum-likelihood phylogenies: assessing the performance of PhyML 3.0. *Syst Biol* 59:307–321. <https://doi.org/10.1093/sysbio/syq010>
79. Mell JC, Shumilina S, Hall IM, Redfield RJ. 2011. Transformation of natural genetic variation into *Haemophilus influenzae* genomes. *PLoS Pathog* 7:e1002151. <https://doi.org/10.1371/journal.ppat.1002151>
80. Collins C, Didelot X. 2018. A phylogenetic method to perform genome-wide association studies in microbes that accounts for population structure and recombination. *PLoS Comput Biol* 14:e1005958. <https://doi.org/10.1371/journal.pcbi.1005958>
81. Li H, Handsaker B, Wysoker A, Fennell T, Ruan J, Homer N, Marth G, Abecasis G, Durbin R. 2009. 1000 genome project data processing subgroup, the sequence alignment/map format and SAMtools. *Bioinformatics* 25:2078–2079. <https://doi.org/10.1093/bioinformatics/btp352>
82. Danecek P, Bonfield JK, Liddle J, Marshall J, Ohan V, Pollard MO, Whitwham A, Keane T, McCarthy SA, Davies RM, Li H. 2021. Twelve years of SAMtools and BCFtools. *Gigascience* 10:giab008. <https://doi.org/10.1093/gigascience/giab008>
83. Chang CC, Chow CC, Tellier LC, Vattikuti S, Purcell SM, Lee JJ. 2015. Second-generation PLINK: rising to the challenge of larger and richer datasets. *Gigascience* 4:7. <https://doi.org/10.1186/s13742-015-0047-8>
84. van Vliet AH, Wooldridge KG, Ketley JM. 1998. Iron-responsive gene regulation in a *Campylobacter jejuni* fur mutant. *J Bacteriol* 180:5291–5298. <https://doi.org/10.1128/JB.180.20.5291-5298.1998>
85. Cameron A, Gaynor EC. 2014. Hygromycin B and apramycin antibiotic resistance cassettes for use in *Campylobacter jejuni*. *PLoS One* 9:e95084. <https://doi.org/10.1371/journal.pone.0095084>